

Fourth-order magnetic anisotropy and tunnel splittings in Mn_{12} from spin-orbit-vibron interactions

Mark R. Pederson,^a Noam Bernstein^a and Jens Kortus^b

^aCenter for Computational Materials Science, Code 6390, Naval Research Laboratory, Washington, DC 20375

^bMPi für Festkörperforschung, Heisenbergstr. 1, D-70569 Stuttgart, Germany
(March 22, 2024)

From density-functional-theory (DFT) based methods we calculate the vibrational spectrum of the $Mn_{12}O_{12}(COOH)_{16}(H_2O)_4$ molecular magnet. Calculated infrared intensities are in accord with experimental studies. There have been no ab initio attempts at determining which interactions account for the fourth-order anisotropy. We show that vibrationally induced distortions of the molecule contribute to the fourth-order anisotropy Hamiltonian and that the magnitude and sign of the effect (6.2 K) is in good agreement with all experiments. Vibrationally induced tunnel splittings in isotopically pure and natural samples are predicted.

The possibility that vibrationally induced modifications of the spin-orbit interaction affects magnetic reorientation barriers has not been previously investigated. A simple model captures the physics but quantitative determination of the coupling constants requires computationally demanding DFT methods. A model Hamiltonian for a single uniaxial anisotropic spin coupled to a one-dimensional harmonic oscillator is given by $H = \frac{1}{2} S_z^2 + \frac{1}{2} (P^2 + Q^2) + Q \sum_{ab} S_a S_b$ where a and b are summed over x, y , and z , and $\frac{d}{dQ} = \frac{d}{dQ}$. Completing the square shows the diagonal energy of a harmonic oscillator (j) and spin (M) product state as a function of the magnetic quantum number (M) is given by:

$$E = \frac{1}{2} S(S+1) + \frac{1}{2} M^2 (A + B M^2)^2 \quad (1)$$

with $A = S(S+1)(\frac{1}{xx} + \frac{1}{yy}) = 2$ and $B = \frac{1}{zz}(\frac{1}{xx} + \frac{1}{yy}) = 2$. For this simple case, the interaction between vibrational and spin degrees of freedom always acts to further stabilize each M state but the energy splitting between the $M = S$ and $M = 0$ states may be either enhanced or reduced depending on the derivatives of the matrix. A more detailed analysis of this Hamiltonian, given below, shows that it can also connect M and $M \pm 4$ levels. Further, in a real system, the frequency, ω , depends on nuclear masses so isotope effects can lead to small changes in the barrier or, as discussed below, larger tunnel splittings in the anisotropy Hamiltonian. Both the intrinsic 4th-order and isotope effects can mediate resonant tunneling of magnetization which is of great interest from the standpoint of quantum mechanics at the mesoscale. [16] In addition, the magnitudes of terms in the anisotropy Hamiltonian determine the suitability of nanoscale particles for use in magnetic memory and quantum computing applications. [7,8] In general, purely electronic contributions to higher-order magnetic anisotropy scale as $[L/(2c^2)]^4$ (c = speed of light) but the spin-orbit-vibron contribution scales as $[L/(2c^2)]^4$. The large $L/(2c^2)$ prefactor suggests

this term could be dominant in high-symmetry bulk systems where second-order effects vanish by symmetry.

Recent experiments on $Mn_{12}O_{12}(COO)_2(H_2O)_2$ molecular nanomagnets, commonly referred to as Mn_{12} -Ac, [16,9] provide an ideal system for understanding how vibrational degrees of freedom may enhance the magnetic barriers. Many researchers have noted that the tunneling dynamics may be mediated by conventional spin-phonon interactions. [10] Further, recent experiments by Sushkov et al. [9] show some strong variation in infrared (IR) spectra as a function of applied field suggesting a coupling between the spin and vibrational degrees of freedom. Accurate experiments have determined that this easy-axis uniaxial molecular magnet has a second-order anisotropy parameter of $D = 0.56$ K and that the fourth-order contributions to the anisotropy Hamiltonian increase the barrier from 56 K to approximately 65 K. [3,5,6] Pederson and Kohn have combined DFT, spin-orbit coupling and second-order perturbation theory to calculate the second-order parameter (D) and find $D = -0.557$ K in excellent agreement with experimental measurements. [11] An estimate of the entirely electronic spin-orbit-induced fourth-order anisotropy may be obtained by comparing the barrier computed with spin-orbit treated within second-order perturbation theory to that computed using exact diagonalization. Within this approach we find a fourth-order contribution to the barrier on the order of 1 K and that it acts to reduce rather than to enhance the barrier.

To determine if vibrational coupling is an important contribution to magnetic anisotropies in Mn_{12} -Ac we have performed accurate DFT based calculations on a single molecular unit. The Perdew-Burke-Ernzerhof generalized-gradient approximation has been used for all calculations. [12] Using the methods discussed in Ref. [13], the vibrational frequencies, vibrational eigenvectors, and IR and Raman spectra have been calculated. Because this requires a large number (163) of unsym-

metrized molecular calculations we have used a Troullier-Martins type [14,15] pseudopotential for the O and C atoms and have treated the H and Mn atoms within an all-electron method. Gaussian basis sets have been fully optimized for each atom using the methods of Ref. [16]. To determine the anisotropy Hamiltonian and the derivatives with respect to each normal mode, we calculate the anisotropy Hamiltonian $H = \sum_{ab} S_a S_b$ for each of the 163 inequivalent vibrational displacements using the method of Ref. [11]. The coefficients γ_{xy} for an arbitrary configuration of atoms are determined from matrix elements of the spin-orbit-coupling operator sandwiched between all pairs of occupied and unoccupied Kohn-Sham wavefunctions (squared) and appropriate energy difference denominators. The wavefunctions and thus the anisotropy Hamiltonian depend on the geometry of the molecule. Derivatives of the anisotropy matrix with respect to the j^{th} normal mode (i.e. $\frac{d_{ab}}{dQ_j}$) may be determined using a finite-difference approach. We have ascertained that the partial-pseudopotential-based anisotropy Hamiltonian for the equilibrium geometry reproduces the all-electron anisotropy Hamiltonian of Ref. [11]. To test the accuracy of the vibrational frequencies we compare our calculated IR spectra, plotted in Fig. 1, directly to experimental measurements of Sushkov et al. [9]

The experiments measure the IR absorption of Mn_{12} crystals suspended in paraffin pellets at wavenumbers ranging from 30 cm^{-1} to 70 cm^{-1} and from 140 cm^{-1} to 650 cm^{-1} . The experimental absorption peak at 38 cm^{-1} has a clear corresponding feature in our calculations at 63 cm^{-1} . The structure in the 140 cm^{-1} to 300 cm^{-1} range is well reproduced by the calculations: The small experimental peaks at 150 cm^{-1} , 170 cm^{-1} , and 200 cm^{-1} correspond to simulated features at 144 cm^{-1} , 170 cm^{-1} , and 201 cm^{-1} , respectively, and the relative intensities are moderately well reproduced. The small peak in the simulation at 180 cm^{-1} can be tentatively identified in the experiment as a small peak at 185 cm^{-1} . The structure between 215 cm^{-1} and 235 cm^{-1} in the experiment, consisting of a large peak, a small peak, and a large peak with a shoulder at high frequency, has a clear analogue in the simulation results between 230 cm^{-1} and 260 cm^{-1} with similar relative intensities. The intense peak at 255 cm^{-1} corresponds to the simulation peak at 275 cm^{-1} , with the smaller experimental peak at 270 cm^{-1} appearing in the simulation as a shoulder at 260 cm^{-1} . The double peaked structure observed in experiment at 284 cm^{-1} , which has significant activity in a magnetic field, corresponds to the simulated peaks at 302 cm^{-1} , 313 cm^{-1} and 316 cm^{-1} . The following experimental triplet, consisting of a large peak at 300 cm^{-1} followed by two small peaks at 320 cm^{-1} and 340 cm^{-1} , is present in the simulation, although at the resolution of the graph in Fig. 1 the two peaks at 326 cm^{-1} and 329 cm^{-1} overlap, and the third peak ap-

pears at 343 cm^{-1} . The small peak at 360 cm^{-1} and intense peak at 375 cm^{-1} are reproduced in the simulation with opposite relative intensities (or interchanged frequency order) in the double peaked structure at 360 cm^{-1} to 368 cm^{-1} . The intense peak at 410 cm^{-1} bracketed by two smaller peaks at 395 cm^{-1} and 415 cm^{-1} appears in the simulation between 412 cm^{-1} and 439 cm^{-1} . The two small peaks in the calculated IR spectrum at 385 cm^{-1} and 395 cm^{-1} are not clearly visible in the experimental data, although they could correspond to the small feature at 382 cm^{-1} to 390 cm^{-1} in the gap between the prominent double peak and triple peak structures. In the highest frequency range measured by experiment agreement with the simulation is still good, although the relative intensities of the peaks are less accurately reproduced. The two faint experimental peaks at 465 cm^{-1} and 495 cm^{-1} probably correspond to the two relatively prominent peaks at 460 cm^{-1} and 476 cm^{-1} . The peaks between 510 cm^{-1} and 570 cm^{-1} correspond to the peaks between 500 cm^{-1} and 545 cm^{-1} . Although the intensities relative to the previous two peaks are lower in the simulation, opposite to experiment, the relative intensities within the peak structure are good. In both the experiment and simulation the second and fifth peaks are most prominent. The intense double peak at 605 cm^{-1} to 610 cm^{-1} clearly corresponds to the simulated double peak at 564 cm^{-1} to 571 cm^{-1} . There is no comparably intense feature in the simulation that corresponds to the highest frequency experimental peak at 640 cm^{-1} , although several less intense peaks are present in the correct frequency range.

The decomposition into contributions from different structural elements in the Mn_{12} molecule shows some general trends as a function of frequency, but no sharp variation from mode to mode. Below 500 cm^{-1} , the main contributions are from the Mn and formic acid. The water molecules contribute mainly for modes below about 350 cm^{-1} , while the anionic oxygen atoms contribute mainly above this frequency. Above 500 cm^{-1} the Mn contribution grows relative to the formic acid contribution, with particularly large Mn and anionic oxygen weights in the 564 cm^{-1} to 571 cm^{-1} double peak.

We now discuss our calculations on the vibrational contributions to fourth-order anisotropy. The coupled spin/vibron Hamiltonian is given by:

$$H = \sum_{ab} S_a S_b + \sum_j \frac{1}{2} P_j^2 + \sum_j \frac{1}{2} Q_j^2 + \sum_{ab} \frac{2}{j} \frac{d_{ab}}{dQ_j} Q_j S_a S_b \quad (2)$$

The above expression may be analyzed either classically or quantum-mechanically to determine how vibrational coupling affects the magnetization barrier. As demonstrated below the magnetization barrier is enhanced by

approximately 5.6 K classically and 6.2 K quantum mechanically since the quantum mechanical expectation value of S^2 is 10 % larger than the classical value for $S=10$. However, to address questions related to isotopic effects and changes in tunnel barriers a quantum mechanical analysis is required.

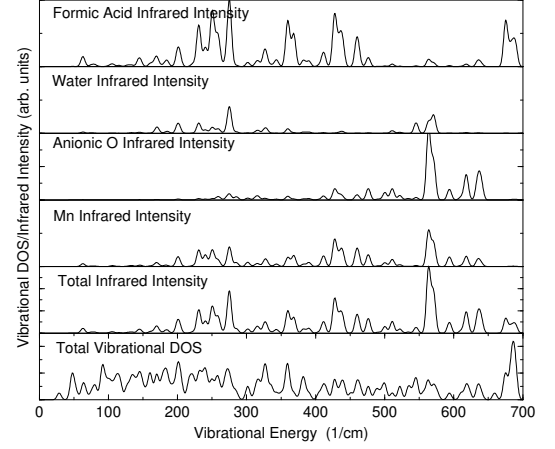
The simplest level of approximation is to take a product wavefunction of the form $\psi_i = \psi_j \psi_i \psi_M$, with ψ_j a harmonic oscillator wavefunction and ψ_M a spin-wavefunction, and determine the diagonal energy of this state. The resulting energy $E(M) = \langle \psi_M | \hat{H} | \psi_M \rangle$ is given by:

$$E(M) = \sum_{ab} U^{ab}(M) + \sum_j \frac{1}{2} \sum_{abcd} U^{ab}(M) U^{cd}(M) \quad (3)$$

with $U^{ab} = \frac{P}{j! 2^{j/2}} \frac{d^j U^{ab}}{dQ^j} \frac{d^j \psi_0}{dQ^j}$; and $U^{ab} = \langle \psi_M | \hat{S}_a \hat{S}_b | \psi_M \rangle$. The 4th-order barrier enhancement may then be estimated by evaluating the second line of Eq. (3) for the $M = 10$ and $M = 0$ states and taking the difference. This energy difference is 6.2 K.

To compare directly to the experimental parameterization of Barra et al. which uses 4th-order Stevens operators, it is instructive to expand both our calculated and their fitted 4th-order expression in terms of orthogonal cubic polynomials of degree 4. Because of the S_4 symmetry of the molecule, it is generally possible to write the fourth-order energy according to: $E^4 = A_0^4 + (A_1(4) [S_z^2 - S^2/3]) + A_2(4) [3S_x^4 + 35S_z^4 - 30S_x^2 S_z^2] + B_1(4) [S_x^4 + S_y^4 - 6S_x^2 S_y^2] + B_2(4) [S_x S_y (S_x^2 - S_y^2)] = 10^4$. In Table I, we compare the values of the expansion coefficients for each representation. The O_4^2 Stevens operator can be expanded into Legendre polynomials of degree 2 and 4 respectively.

An interesting feature, present in both the experimental and theoretical expansions, is that for the most part, the 4th order terms exhibits nearly the same angular variation as the second-order Hamiltonian. For example the entirely diagonal 4th order $S^2 (S_z^2 - S^2/3)$ term accounts for almost all of the barrier enhancement. This feature is very important from the standpoint of sharp tunneling transitions. It ensures that magnetic-field induced alignment condition aligns multiple pairs of states simultaneously which opens multiple tunneling paths. The coefficient $A_2(4)$ changes the diagonal energies by $A_2(4) M^4 = 10^4$ and is partially responsible for a broadening of the magnetic-field alignment condition but does not cause any tunnel splittings at zero-field. The $B_1(4)$ coefficient corresponds to the B_4^4 Stephenson coefficient, and leads to observable tunnel splittings in the $M = 2$ manifold and smaller tunnel splittings in the $M = 4$ manifold. Our isotopically pure calculations show tunnel splittings of the $M = 2$, $M = 4$, and $M = 6$



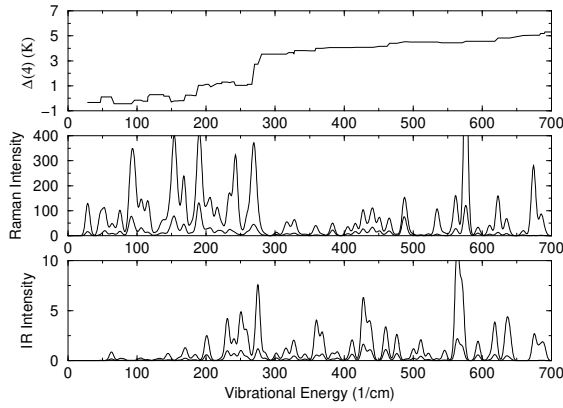
Pederson LN8174 Fig 1

FIG. 1. Calculated total and IR vibrational density of states for the Mn_{12} molecule. In addition we have projected the IR active density of states onto Mn, O^2 , $COOH$, and H_2O to show the origin of the IR spectrum.

manifolds of approximately 10^{-2} , $7 \cdot 10^{-6}$ and $6 \cdot 10^{-10}$ K respectively but do not split the odd M states since coupling is between M and $M \pm 4$. By randomly changing a single atomic mass by 1 amu, we find that the odd- M states are split with a tunnel splitting of the $M = 1$ states on the order of 10^{-4} K. The isotopic effects experimentally observed by Wernsdorfer et al. [17] in Fe_8 may be partially due to the mass effects identified here.

In Fig. 2 we show the barrier as a function of the number of vibrational modes that are included. When none of the vibrational modes are included the barrier reproduces the earlier calculation of Ref. [11]. As expected qualitatively, most (85 %) of the fourth-order barrier is associated with the frequencies in the $100\{500 \text{ cm}^{-1}$ range that correlates with Mn vibrations. The upper panel of the figure shows that there are a 5{10 modes which account for about 80{90 % of the fourth-order anisotropy barrier. For example, single modes at 189, 270, 280, and 465 and 1496 cm^{-1} contribute 0.8 K, 1.6 K, 0.8 K, 0.25 K and 0.45 K respectively to the 4th-order barrier. These modes and all other modes that contribute visible spikes in Fig. 2 share one simple trait. They are optically silent to IR absorption and transmission but show strong Raman intensity. The calculated Raman intensities for these modes are shown in Table II.

Recently, Sushkov et al. [9] have performed experiments on Mn_{12} -Ac and have shown that the IR transmissions at 284, 306 and 409 cm^{-1} exhibit strong dependencies when magnetic fields are applied to the crystal and that the dependence is particularly strong for the mode at 284 cm^{-1} . This suggests that vibrations in this energy range are associated with the spin carrying Mn ions as confirmed from the projected DOS in Fig. 1. While the Raman modes are responsible for the form-



Pederson LN8174 Fig2

FIG. 2. Evolution of 4th order anisotropy barrier ($\Delta(4)$) as a function of the number of modes included. Also shown is the total and Mn-projected calculated IR and Raman spectra. Large jumps in the barrier are due to strong Raman modes, as discussed in the text.

tion of the 4th-order barrier, the strong contributions due to Mn motion at 270 and 280 cm^{-1} is qualitatively consistent with the strong field-dependent IR dependencies observed experimentally in this energy range.

TABLE I. Calculated Raman intensities for modes that are primarily responsible for the formation of the vibrational 4th-order magnetic anisotropy. Units of Raman intensities are respectively $\text{Å}^4/\text{amu}$.

ν (cm^{-1})	Raman	4th-order shift (K)
189	297	0.8
270	508	1.6
281	24	0.8
465	263	0.25
1496	5400	0.45

TABLE II. Fourth-order anisotropy Hamiltonian as determined from experiment, DFT plus vibration-spin coupling, and DFT without this coupling. For simplicity we have reexpanded the representation of Barra et al. in terms of orthogonal cubic polynomials rather than the Stephens polynomials used in their work. All numbers are given in $\text{K} \cdot 10^4$.

	$A_1(4)$	$A_2(4)$	$B_1(4)$	$B_2(4)$
Experiment	-8.35	-0.334	-0.43	0.000
Vibrational	-5.58	-0.008	-0.01	-0.015
Electronic	0.68	0.0005	-0.002	0.004

While the calculated 4th-order contribution to the tunneling barrier of 6.2 K is in close agreement with the experimental values of 7(10) K, it is indeed a small number so it is appropriate to consider other vibrational effects that might be nonnegligible.

To determine possible effects of methyl termination of the carboxyl groups, we have changed the mass of the

H on the formate groups from 1 to 15 (the mass of a CH_3). This further increases the 4th-order anisotropy from 6.2 K to 7.3 K and leads to even better agreement with experiment. There could also be terms due to $d^2 = dQ^2$. However, such interactions effectively change the vibrational spring constant and scale as $\frac{2}{M \cdot \Gamma^4}$ rather than $\frac{4}{\Gamma^2 \cdot c^8}$ where Γ is the total magnetic moment. Because of the large masses involved (even for hydrogen) an order of magnitude estimate suggests that the total barrier would change by less than 0.01 K from this type of effect. Further, in contrast to terms discussed above, these contributions add as amplitudes and could partially cancel one another. The spring-constant terms directly modify the 2nd-order matrix allowing for isotopic induced symmetry breaking. While potentially unimportant from the standpoint of barrier formation, this effect leads to a type of locally varying second-order transverse anisotropy required to explain experiments (See Ref. [18].) We are in the process of studying this and other possibilities.

To summarize, we have performed accurate DFT-based calculations on the $\text{Mn}_{12}\text{-Ac}$ molecule to determine whether vibron-spin coupling could be responsible for part of the 4th-order anisotropy Hamiltonian. Our results suggest that vibron-spin coupling accounts for most of the effect and that it is significantly larger and a different sign than the $O(1/c^8)$ terms that arise from an exact diagonalization treatment of spin-orbit coupling.

This work was supported in part by ONR grant N0001400W X20111 and N0001401W X31303.

-
- [1] R. Sessoli, D. Gatteschi, A. Caneschi and M. A. Novak, Nature 365 141 (1993).
 - [2] A. Caneschi, D. Gatteschi, C. Sangregorio, R. Sessoli, L. Sorace, A. Comia, M. A. Novak, C. Paulsen and W. Wernsdorfer, J. Magnetism and Magnetic Mat. 200, 182 (1999) and references therein
 - [3] J. Friedman, M. P. Sarachik, J. Tejada, J. Maciejewski and R. Ziolo, Phys. Rev. Lett. 76, 3820 (1996) L. Thomas, F. Lioni, R. Balbu, D. Gatteschi, R. Sessoli and B. Barbara, Nature (London) 383, 145 (1996);
 - [4] C. Sangregorio, T. Ohm, C. Paulsen, R. Sessoli and D. Gatteschi, Phys. Rev. Lett. 78, 4645 (1997).
 - [5] A. L. Barra, D. Gatteschi and R. Sessoli, Phys. Rev. B 56 8192 (1997).
 - [6] F. L. Mettes, F. Luis and L. J. de Jongh, Phys. Rev. B 64, 174411 (2001).
 - [7] S. Sun, C. B. Murray, D. Weller, L. Folks, and A. Moser, Science 287, 1989 (2000).
 - [8] M. N. Leuenberger and D. Loss, Nature 410, 789 (2001).
 - [9] A. B. Sushkov, B. R. Jones, J. L. Musfeldt, Y. J. Wang, R. M. Acheson and N. S. Dalal, Phys. Rev. B 63, 214408 (2001).

- [10] A. Garg, Phys. Rev. Lett. 81, 1513 (1998).
- [11] M. R. Pederson and S. N. Khanna, Chem. Phys. Lett. 307, 253, (1999); *ibid.* Phys. Rev. B 60, 9566 (1999).
- [12] J. P. Perdew, K. Burke and M. Ernzerhof, Phys. Rev. Lett. 77, 3865 (1996).
- [13] D. Porezag and M. R. Pederson, Phys. Rev. B 54, 7830 (1996).
- [14] N. Troullier and J. L. Martins, Phys. Rev. B 43 1993 (1991).
- [15] D. Porezag, M. R. Pederson and A. Y. Liu, Phys. Rev. B 60, 14132 (1999).
- [16] D. Porezag and M. R. Pederson, Phys. Rev. A 60, 2840 (1999).
- [17] W. Wemsdorfer et al, Phys. Rev. Lett. 84, 2965 (2000).
- [18] K. M. Mertes et al, Phys. Rev. Lett. 87, 227205 (2001).